PL-TR--91-3059

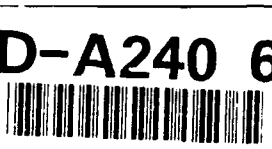

PL-TR--
91-3059

(2)

DECOMPOSITION PATHWAYS OF TETRAHYDROGEN

William A. Lester, Jr.

University of California, Berkely
Sponsored Projects Office,
Banway Building
Berkely, CA 94720

August 1991

Final Report

PHILLIPS LABORATORY
Propulsion Directorate
AIR FORCE SYSTEMS COMMAND
EDWARDS AIR FORCE BASE CA 93523-5000

NOTICE

When U.S. Government drawings, specifications, or other data are used for any purpose other than a definitely related Government procurement operation, the fact that the Government may have formulated, furnished, or in any way supplied the said drawings, specifications, or other data, is not to be regarded by implication or otherwise, or in any way licensing the holder or any other person or corporation, or conveying any rights or permission to manufacture, use or sell any patented invention that may be related thereto.

FOREWORD

This final report was submitted by the University of California, Berkeley, Berkely CA on completion of contract F04611-87-K-0030 with the OLAC, Phillips Laboratory (AFSC), Edwards AFB CA 93523-5000. OLAC PL Project Manager was Dr. Stephen L. Rodgers.

This report has been reviewed and is approved for release and distribution in accordance with the distribution statement on the cover and on the SF 298 .

Stephen L. Rodgers

STEPHEN L. RODGERS
Chief, Emerging Technologies Branch

RANNEY G. ADAMS
Public Affairs Director

FOR THE COMMANDER

David W. Lewis

DAVID W. LEWIS, MAJOR, USAF
Acting Director
Fundamental Technologies Division

REPORT DOCUMENTATION PAGE

Form Approved
OMB No. 0704-0188

1. AGENCY USE ONLY (Leave blank)	2. REPORT DATE	3. REPORT TYPE AND DATES COVERED
	Aug 91	Final Jul 87 to Dec 90

4. TITLE AND SUBTITLE
Decomposition Pathways of Tetrahydrogen

5. FUNDING NUMBERS
C - F04611-87-K-0030
PR- 5730
PE- 002H
WU- 344661

6. AUTHOR(S)
William A. Lester, Jr.

7. PERFORMING ORGANIZATION NAME(S) AND ADDRESS(ES)
The Regents of the University of California
University of California, Berkeley
Sponsored Projects Office
Banway Building
Berkeley, CA 94720

8. PERFORMING ORGANIZATION REPORT NUMBER

9. SPONSORING/MONITORING AGENCY NAME(S) AND ADDRESS(ES)
Phillips Laboratory
Propulsion Directorate
Edwards AFB, Ca 93523-5000

10. SPONSORING/MONITORING AGENCY REPORT NUMBER
PL-TR-91-3059

11. SUPPLEMENTARY NOTES
COSATI Codes: 12/03, 07/02, 07/02.

12a. DISTRIBUTION/AVAILABILITY STATEMENT
Approved for Public Release; distribution is unlimited.

12b. DISTRIBUTION CODE

13. ABSTRACT *(Maximum 200 words)*

Investigations of a variety of possible decomposition pathways using quantum Monte Carlo methods including a careful examination of nonadiabatic couplings between excited and the ground state using state-averaged multiconfiguration self-consistent field procedures lead to the conclusion that the H_4 MIES is a very short lived species.

Minimum energy paths have been computed for use in constructing improved ground and excited potential energy surfaces for the calculation of reorientation cross sections for He + $H_2(B\ ^1\Sigma_u^+)$.

14. SUBJECT TERMS
Tetrahydrogen; decomposition pathways; nonadiabatic coupling; Helium/Singlet B Hydrogen

15. NUMBER OF PAGES
48

16. PRICE CODE

17. SECURITY CLASSIFICATION OF REPORT	18. SECURITY CLASSIFICATION OF THIS PAGE	19. SECURITY CLASSIFICATION OF ABSTRACT	20. LIMITATION OF ABSTRACT
UNCLASSIFIED	UNCLASSIFIED	UNCLASSIFIED	SAR

NSN 7540-01-280-5500

Standard Form 298 (Rev 2-89)
Prescribed by ANSI Std 239-18
298-102

QUANTUM MONTE CARLO STUDY OF THE DECOMPOSITION

PATHWAYS OF TETRAHYDROGEN

Table of Contents

PART A: QUANTUM MONTE CARLO STUDY OF THE DECOMPOSITION PATHWAYS OF TETRAHYDROGEN

I. Introduction

Bound excited states of small molecules are of both practical and theoretical interest. Stabilized and vacuum-stored excited-state molecules have been postulated as a new energy source. Nicolaides *et al.* have suggested an H_4 species as a candidate system.[1] In their multireference single- and double-excitation configuration interaction (MR-SDCI) study, a species they labeled a maximum ionicity excited state (MIES) of pyramidal geometry with equilateral triangle base was found for which the coulomb attraction between the ionic fragments H_3^+ and H^- governed stability. In their work, a local excited-state minimum was characterized that results from an avoided curve crossing between the lowest-lying $1\ ^1A'$ and $2\ ^1A'$ states.

In experiments by Moore and collaborators, however, large quenching cross sections have been measured for the interaction of excited-state $H_2(B\ ^1\Sigma_u^+) \equiv H_2(B)$ molecule with ground-state $H_2(X\ ^1\Sigma_g^+) \equiv H_2(X)$ molecules.[2] This evidence could be interpreted as an argument against stability of an excited H_4 species. The correlation diagram for the interaction of two H_2 molecules shows that $H_2(B)$ can dissociate to an unstable H_3 and H atom with subsequent decomposition to $H_2 + H + H$ or $H + H + H + H$; see Fig. 1.

To ascertain the stability of various H_4 species requires determination of the possible decomposition pathways. Many *ab initio* potential energy surface (pes) studies of nuclear arrangements of high symmetry have appeared including investigations of the square,[3,4b] rectangle,[3,5] rhombus,[3] trapezoid,[5b,6b] and various tetrahedra.[3,5b] A three-dimensional equipotential map including several of the lowest-lying states for (C_{2v}) tetrahedra have been provided by Michl[5a] *et al.* Various symmetric pathways have been investigated including the (C_{2v}) in-plane "T" approach,[7] "kite" approach,[11] and two perpendicular plane approaches.[5a] In addition, a detailed molecular orbital correlation analysis has been reported.[8]

The major findings of those studies are: (1) the reaction of excited $H_2(B)$ with ground state $H_2(X)$ is exothermic with activation energy; (2) the ground state pes that correlates to $H_2(X) + H_2(X)$ is repulsive and the excited pes that correlates to $H_2(X) + H_2(B)$ is bound and leads to the formation of excimer H_4^*; (3) the binding of the excimer is due to charge transfer; (4) there is either a crossing or avoided crossing between two or more lowest-lying states that provides a funnel facilitating decay of the excited state to the ground state.

Montgomery *et al.* pointed out that the well, implied by a one-dimensional plot in Ref. 1, for the ground $1\ ^1A'$ state is actually a saddle point on the multidimensional surface.[9] Nicolaides *et al.* followed their earlier prediction with a new finding of a minimum

on the excited singlet surface for C_s trigonal pyramidal geometry.[10,11] In the latter papers, nonadiabatic coupling matrix elements that connect the excited- and ground also were reported.

To better understand stability of the excimer H_4 species, tetrahydrogen, a quantum Monte Carlo[12] study of the system was carried out under this contract that also included state averaged multiconfiguration self-consistent field (SA-MCSCF) calculations of nonadiabatic coupling matrix elements over a range of coordinate values to enable a detailed investigation of possible decomposition pathways. Although an extended basis set is required to describe the highly ionic character of H_4 and its dissociation in conventional *ab initio* basis set approaches, QMC routinely yields improved absolute energies with nominal dependence on basis set.[12] Furthermore, our recently developed symmetry constrained optimization technique[13] can easily handle degeneracies that arise in curve crossing (avoided crossing) regions without regard to the particular symmetry type.

The remainder of Part A is arranged as follows. Section II summarizes the central features of the QMC method. Section III presents findings of our MCSCF and QMC survey studies of the one-dimensional pes as a function of separation between apex H and triangular base H_3. This is followed in Sec. IV with results of decomposition pathway explorations. Section V presents and discusses a two-dimensional pes contour map for C_{3v} symmetry. Section VI describes splitting of the ^1E state at deformed (non C_{3v})

geometries and the interaction between these lowest-lying states followed in Sec. VII with consideration of the role of nonadiabatic coupling in the subject system. Section VIII discusses our H_4 results and presents conclusions of the study.

II. Method

Quantum Monte Carlo

QMC is a stochastic method for solving the Schrödinger equation by a random walk process. An attractive feature of QMC is that with modest basis sets and single or small multiconfiguration wavefunctions combined with electron correlation factors that are explicit functions of interelectronic distance, one often recovers 90-100% of the correlation energy.[14-25]

Because QMC is well described elsewhere,[12] we present only a brief summary adequate for present purposes. Introducing $f \equiv \psi\psi_t$ where ψ is the exact eigenfunction of the N-electron system Hamiltonian and ψ_t is a trial (approximate) wavefunction, the time-dependent Schrödinger equation in imaginary time τ can be written

$$-\frac{\partial f}{\partial \tau} = -\frac{1}{2} D\nabla^2 f + D\nabla\cdot F_D f + (E_L - E_t) f \quad . \tag{1}$$

Here $D \equiv \hbar^2/2m_e$ where m_e is the electron mass and E_t is a constant shift of the zero of energy. Monte Carlo sampling of Eq. (1) in 3N-dimensional space is governed by three factors corresponding to the three terms on the right-hand side of Eq. (1), namely, (1) diffusion, (2) particle drift under the influence of a "quantum force,"

$$F_D = \nabla(ln\ \psi_t^2) = \frac{2\nabla\psi_t}{\psi_t} \quad , \tag{2}$$

and (3) a first-order kinetic or branching process.

The local energy

$$E_L = \frac{H\psi_t}{\psi_t} \tag{3}$$

is sampled throughout 3N-dimensional space. If one carries out random walks in the absence of the branching process, i.e., variational Monte Carlo (VMC), the usual variational energy is obtained, i.e.,

$$\langle E \rangle_V = \frac{\langle \psi_t | H | \psi_t \rangle}{\langle \psi_t | \psi_t \rangle} \quad . \tag{4}$$

Inclusion of the branching step leads to the fixed-node energy

$$\langle E \rangle_{FN} = \frac{\langle \psi_{FN} | H | \psi_t \rangle}{\psi_{FN} | \psi_t \rangle} \quad . \tag{5}$$

It is well established that Eq. (4) yields an upper bound to the ground-state energy; in Ref. 12 it is shown that Eq. (5) also provides an upper bound.

In this work, the trial function ψ_t was constructed as a product of a single determinant and symmetric two-body (electron-electron and electron-nucleon) correlation factors. These factors were determined as follows.

(a) Determinantal function: a basis set of 25 Slater-type

functions on each atom, consisting of two 1s (1.68, 0.8) and single 2s (0.9) and 2p (1.6) functions was used in a MCSCF calculation for a ten-configuration wavefunction formed by allowing two electrons to be singly and doubly excited among four molecular orbitals (MO). The term with the largest coefficient (>0.985) was selected as the independent-particle function.

(b) Two-body correlation factors: the familiar Jastrow function[26]

$$G = \prod_{i,a} G_{ia}$$

where

$$G_{ia} = exp\left(\frac{ar_{ia}}{1+br_{ia}}\right) \tag{6}$$

was used to describe electron-nucleon (e-n) correlation. Here r_{ia} denotes the separation between the i-th electron and a-th nucleus. A related but improved form[27]

$$S = \prod_{i>j} [1 - \alpha_1 exp(- r_{ij}/b_1) - r_{ij}^2/b_2)] \tag{7}$$

was introduced to represent electron-electron (e-e) correlation where r_{ij} is the separation between electrons i and j.

(c) Optimization: with the introduction of correlation factors, it is desirable to optimize the product function, i.e., the linear and nonlinear coefficients of the determinant as well as the correlation parameters a, b, as well as a_1, b_1, and b_2. This was readily achieved with a recently reported algorithm.[13] In order

to maintain the symmetry of the state under consideration and to retain orthogonality between different states, a group theoretic symmetry constraint is enforced during optimization. This takes the form of a point group projection operator for the MOs and a Young tableaux permutation group projection operator to insure proper multiplets. (This capability was developed under support by this contract.)

III. Potential Energy Surface for C_{3v} Symmetry

For C_{3v} symmetry, potential curves for the three lowest-lying states, i.e., the doubly degenerate ^1E state and the $^1A_1$ state were computed as a function of separation R between the apex H atom and the equilateral triangle base of H atoms. The triangle side-length r was fixed for two sets of calculations at 1.70 a.u. and 1.80 a.u. These results are presented in Figs. 2 and 3, respectively. At each point the independent-particle function was taken either as the lead term from a MCSCF calculation or from a previously optimized function at an adjacent geometry. Optimization of the product of single-particle and correlation functions was carried out subject to the symmetry constraint mentioned in Sec. II. The constraint facilitates the capability of distinguishing states in the curve crossing region where near degeneracy often causes root flipping in MCSCF calculations.

The potential curves of Fig. 2 for r = 1.70 a.u. were generated by a least-squares fitting procedure to 18 QMC energies. At R = 6.0 a.u. the QMC ground-state (^1E) energy is −2.0650(30)

which is in good agreement with the sum of the asymptotic H_3 ground-state energy (−1.565 a.u.[28]) plus H atom energy (−0.5 a.u.). Note that the QMC curve crossing at R = 3.9 occurs at a slightly larger distance than that found in the Nicolaides *et al.* study[1] reproduced in Fig. 2 by the dotted line. In most regions the QMC results are lower by 0.6-1.0 eV. This considerable energy lowering prompted us to carry out a singles and doubles configuration interaction (SDCI) calculation which was done at R = 3.4 a.u. The energy obtained was −2.059 a.u. which lies, as anticipated, between the results of Nicolaides *et al.* and the present QMC energy and provides a consistency check.

In Fig. 3 QMC energies are displayed resulting from QMC calculations at 16 geometries, ranging from R = 3.0 to 6.0 a.u. for r = 1.80 a.u. for the doubly degenerate ^1E state and the $^1A_1$ states. The components of the ^1E state were calculated independently using the symmetry constraint method[13] mentioned in Sec. II. The closeness of the energies of the components confirms that the ground state, as the correlation diagram analysis indicates, is doubly degenerate. Curve crossing occurs at R = 4.3 a.u. which is larger than the distance found at r = 1.70 a.u. Compared with results at r = 1.70 a.u., one finds a shift in the shape (as characterized by the onset of repulsion) of the potential curve to smaller R as would be anticipated because of the larger separation of the H atoms forming the base of the pyramid.

IV. Approach of $H_2(B)$ and $H_2(X)$

Calculations were performed for $H_2(B)$ approach to $H_2(X)$ in which these molecules are contained initially in perpendicular bisector planes; see Fig. 4. Table 1 summarizes the sequence of geometry changes, labeled I-VIII, that were followed to carry the system from the asymptotic region to the neighborhood of the H_4 MIES configuration. The table also lists the energy lowerings associated with the steps which are plotted in Fig. 5. It is noteworthy that no energy barrier is encountered along this path. Further, Fig. 6 shows that when $H_2(B)$ is displaced from bisecting $H_2(X)$ in Step II, charge transfer occurs immediately. (Similar behavior has been found for the related $H_2(B)$ + He system in an independent study by the P.I.)

Calculations to explore the possibility of dissociation via paths alternative to the pyramidal MIES avenue have also been carried out. One possibility is the so called T-approach pathway in which $H_2(X)$ approaches $H_2(B)$ in a C_{2v} T configuration. Over a wide range of geometries, no barrier was found, see Table 2. The excited state energy E_2, however, did drop below the MIES energy (−2.065 a.u.) reported in the previous section. But the interaction at shorter separations remains to be explored. The interesting finding is that charge transfer ends before curve crossing occurs.

V. Two-dimensional Energy Surface with C_{3v} Symmetry

Figures 6 and 7 show contour maps constructed using a 28-

configuration MCSCF wavefunction and the basis set of Sec. II. MCSCF calculations at 125 geometries and QMC computations at 49 geometries were performed for r = 1.55-2.00 a.u. and R = 3.0-5.4 a.u. The ^1A state (Fig. 7) and doubly degenerate ^1E state (Fig. 8) surfaces were found to cross along a seam represented by the dashed line in each figure. A noteworthy feature is that the seam is nearly linear. It is described well by the relation R = −4.7166 r + 1.2594. In both cases the minimum energy along this seam is found at r = 1.80 a.u. and R = 4.1453 a.u., near the point where the seam is tangential to the E = −2.000 a.u. contour.

As shown previously, QMC calculations of this system can lead to total energies 2-2.5 eV lower than MCSCF calculations with a double-zeta plus polarization (DZP) basis set. It has also been documented that QMC results are weakly dependent on the basis set used to construct the QMC trial function. For these reasons, it was important to revisit the two-dimensional potential energy surface discussed above with the QMC method. Using the optimization algorithm and the symmetry constraint technique we constructed[13] a MCSCF trial function for the QMC calculations. MCSCF energies and QMC energies obtained with the MCSCF trial function are listed in Table 3 at nine geometries along the seam. The QMC energies are lower than the MCSCF energies by 1.47-1.97 eV.

These results show that there is a broad crossing region of the three states where nonadiabatic coupling can be significant. Based on present findings it is clear that the excited pyramidal H_4

holds the prospect of decay over a wide range of geometries besides C_{3v} symmetry. Motions that destroy C_{3v} symmetry provide additional pathways for decay of the system.

VI. SA-MCSCF Study of Distorted (non C_{3v}) Geometries

For pyramidal H_4, the structure of the pes's in the vicinity of C_{3v} geometry is more complicated than a conical intersection because there are three, rather than two, surfaces that cross. Our investigation of non C_{3v} geometries consisted of (1) deforming the H_3 base from an equilateral to an isosceles triangle, and (2) displacement of the apex H atom from the peak of the pyramid while retaining the isosceles base. The study proceeded in two parts: (1) Consideration initially of only the states of the same symmetry, thereby ignoring the third state which correlates with the antisymmetric branch of the ^1E state for C_{3v} symmetry. (2) Treatment of all three states at selected geometries.

Perspective view and contour map

Figure 8 provides perspective views and Fig. 9 shows the contour map of the ground and excited pes's at R = 3.8 a.u. From the contour map one sees (1) the local minimum of the excited state does not occur for C_{3v} symmetry, but for an isosceles base arrangement with longer equal-length sides (A) and a shorter third side (B) and (2) the saddle point (S) of the ground state and the local minimum (D) of the excited state are found at different geometries.

These phenomena are explainable by the Jahn-Teller effect.

When a non-symmetric displacement of the nuclei occurs, the symmetry is lowered with loss of the degeneracy. In the present case the degeneracy of the open shell ^1E is broken. As mentioned above Nicolaides *et al.* found a minimum for a deformed geometry[10] consistent with the present findings. Our calculations also found that the energy of the excited state is lowered by a lateral displacement of the apex H atom of 0.1 a.u. along the perpendicular bisector plane of side B towards B.

Strong interaction between three lowest-lying states

Starting with C_{3v} symmetry (see the contour map of the ^1A state in Fig. 6 and the ^1E state in Fig. 7), we calculated the three lowest-lying pes's for R fixed at 4.2 a.u., B held constant, while varying the equal side lengths (A). One-dimensional pes's for B = 1.55-1.95 and A = 3.0-5.4 a.u. were computed. The case B = 1.6 a.u. is plotted in Fig. 10. The calculations were done using the 28-configuration MCSCF wavefunction.

Figure 10 plots the splitting of the two $2^1A'$ and $1^1A''$ branches for A ≠ B. One can observe that the symmetric $2^1A'$ branch interacts strongly with the ground $1^1A'$ state, as expected, since both states have the same symmetry in C_s symmetry. These curves are seen to approach closely at a = 1.70 a.u. although the energy gap between the ^1E and $^1A_1$ states is large (0.696 eV) for C_{3v} symmetry. As the energy gap decreases with increase of b, the interaction is found to increase.

Our findings may be summarized as follows. In addition to the

seams in C_{3v} symmetry, at lower C_s symmetry additional regions of crossing (avoided crossing) are encountered. This is due to splitting of the doubly degenerate ^1E state under geometry deformation and very strong interaction of the symmetric branch with the ground $^1A_1$ state. These findings lend further support to our indications of the lack of stability of the tetrahydrogen system and the prediction of many decay paths.

VII. Nonadiabatic coupling

To estimate the transition probability between the $^1A_1$ state and one of the doubly degenerate ^1E states, five geometries near the crossing region in C_{3v} symmetry have been selected to examine the dependence of the nonadiabatic coupling matrix elements on nuclear displacements. Both the perturbed and unperturbed wavefunctions for these states can be written

$$|A\rangle = \sum_k C_{Ak} \Psi_k^{CSF} \tag{8}$$

$$|E\rangle = \sum_k C_{Ak} \Psi_k^{CSF} \tag{9}$$

$$|A'\rangle = |A\rangle Q = Q' = \sum_k C'_{Ak} \Psi_k^{CFS} \tag{10}$$

$$|E'\rangle = |E\rangle Q = Q' = \sum_k C'_{Ek} \Psi_k^{CFS} \tag{11}$$

where ϕ_k^{CSF}'s are configuration state functions, i.e.,

$$\Psi_k^{CSF} = det|\phi_1 \ldots \phi_n|_k \tag{12}$$

and the molecular orbital function ϕ_j is a linear combination of atom-centered Slater functions

$$\phi_j = \sum_m d_{jm} X_m \tag{13}$$

Here Q and Q' (see Eq. 10) are unperturbed and perturbed nuclear coordinates, respectively. The nonadiabatic coupling matrix elements consist of two terms, one arising from the CI coefficients and the other from the atom-centered basis functions.

$$\langle A|\nabla|E\rangle = D^{CI} + D^{AO} \tag{14}$$

$$D^{CI} = \sum_{kh} C_{Ak} C'_{Eh} \delta_{kh} = \sum_k C_{Ak} C'_{Ek} \tag{15}$$

$$D^{AO} = \sum_{ij} P_{AE}^{ij} \langle \chi_i | \frac{\partial \chi_j}{\partial Q} \rangle \tag{16}$$

Using a triple-zeta plus polarization (TZP) basis set from a previous QMC calculation, a state-averaged MCSCF calculation was carried out to generate 24 reference MOs. A SDCI calculation consisting of 1035 configurations was carried out using both unperturbed (Q) and perturbed (Q') to obtain the CI coefficients (Eqs. 8-11). The atomic orbital term D^{AO} was found to give a very small contribution.

The nonadiabatic coupling matrix elements for each geometry were calculated for the six normal modes of nuclear motion shown in

Fig. 11. Among these modes, Q_3 and Q_6 are A-type (totally symmetric) motions, Q_1 and Q_2 are dissociative E-type motions with imaginary vibrational frequencies, and Q_4 and Q_5 are E-type with real vibrational frequencies.

Representative NA coupling matrix elements are listed in Table 4 for selected r and R. Because of selection rules, the two A-type motions Q_3 and Q_6 make no contribution to the coupling matrix elements. Among the four E-type motions Q_1 and Q_2 (dissociate) lead to strong couplings whereas, Q_4 and Q_5 induce relatively weak couplings.

In the region of closest approach (r = 1.9 a.u., R = 4.6 a.u.) the coupling is very strong. The calculated matrix elements roughly describable by a linear relation vs. the inverse of the energy gap between the $^1A_1$ and ^1E states see Fig. 12.

From our investigation, it is clear that there are a variety of regions (C_{3v} and deformed) where the three lowest-lying pes's have crossings or avoided crossings. In this section we have shown that certain types of nuclear motions cause very strong coupling between these states which provides further evidence for strong quenching and a short lifetime for excited H_4.

VII. Conclusions of the H_4 Study

QMC and MCSCF studies of one-dimensional and two-dimensional pes's show that three states, a doubly degenerate $^1E(C_{3v})$, which splits into $^1A'$ and $^1A''$ (C_s), and a $^1A_1$ state are involved in quenching of excited H_4. In the vicinity of the MIES, that is for

R between 3.0-5.4 a.u. and r between 1.55-2.00 a.u., these states have many crossings or avoided crossings. The splitting of degenerate states and the interaction among these states imply high probability for electronic transitions. The nonadiabatic coupling matrix element calculations showed that the two dissociative E-type normal modes lead to very strong coupling between the $^1A_1$ and ^1E states. Collectively, these findings lead to the prediction that the H_4 MIES is a very short lived species.

References

1. C. A. Nicoladies, G. Theodorakopoulos, and I. D. Petsalakis, J. Chem. Phys. **80**, 1705 (1984); **80**, 1900 (1984); **84**, 748 (1984).
2. E. H. Fink, D. L. Akins, and C. B. Moore, J. Chem. Phys. **56**. 900 (1972).
3. M. Rubinstein and I. Shavitt, J. Chem. Phys. **51**, 2014 (1969).
4. a) J. B. Anderson, J. Chem. Phys. **65**, 4121, (1976); a) Int. J. Quan. Chem. **XV**, 109 (1979).
5. a) W. Gerhartz, R. D. Poshusta, and J. Michl, J. Am. Chem. Soc. **98**, 6427 (1976); b) **93**, 4263 (1977).
6. a) J. D. Goddard and I. G. Csizmadia, Chem. Phys. Lett. **43**, 73 (1976); b) **64**, 219 (1979).
7. E. Kassab, E. M. Evleth, G. Chambaud, and B. Levy, vol. II, pp. 1307, *Photochemistry and Photcbiology*, ed. by A. H. Zewail, Hardwood Academic, New York, 1983.

8. E. M. Evleth and E. Kassab, J. Chem. Phys. **89**, 3928 (1988).

9. J. A. Montgomery, Jr. and H. H. Michels, J. Chem. Phys. **86**, 5882 (1987).

10. A. Metropoulos and C. A. Nicolaides, J. Phys. B: At. Mol. Opt. Phys. **21**, L77 (1988).

11. G. Theodorakopoulos, I. D. Petsalakis, and C. A. Nicolaides, J. Mol. Struc. (Theochem) **149**, 23 (1987).

12. P. J. Reynolds, D. C. Ceperley, B. J. Alder, W. A. Lester, Jr., J. Chem. Phys. **77**, 5593 (1982).

13. S.-Y. Huang, Z. W. Sun, and W. A. Lester, Jr., J. Chem. Phys. **92**, 597 (1989).

14. J. B. Anderson, J. Chem. Phys. **63**, 1499 (1975); **65**, 4121 (1976).

15. D. M. Ceperley and B. J. Alder, Phys. Rev. Lett. **45**, 566 (1980); Physica B **108**, 875 (1981); J. Chem. Phys. **81**, 5833 (1984).

16. M. A. Lee, K. E. Schmidt, M. H. Kalos, and G. V. Chester, Phys. Rev. Lett. **46**, 728 (1981).

17. J. W. Moskowitz and M. H. Kalos, Int. J. Quantum Chem. **20**, 1107 (1981); J. W. Moskowitz, K. E. Schmidt, M. A. Lee, and M. H. Kalos, J. Chem. Phys. **76**, 1064 (1977); **77**, 349 (1982).

18. P. J. Reynolds, M. Dupuis, and W. A. Lester, Jr., J. Chem. Phys. **82**, 1983 (1985).

19. R. N. Barnett, P. J. Reynolds, and W. A. Lester, Jr., J. Chem. Phys. **82**, 2700 (1985).

20. R. J. Harrison and N. C. Handy, Chem. Phys. Lett. **113**, 257 (1985).

21. R. M. Grimes, B. L. Hammond, P. J. Reynolds, and W. A. Lester, Jr., J. Chem. Phys. **85** 4749 (1986).

22. D. R. Garmer and J. N. Anderson, J. Chem. Phys. **86**, 4025 (1987).

23. W. L. McMillan, Phys. Rev. **138**, A422 (1965).

24. D. Schiff, Phys. Rev. **160**, 208 (1967).

25. a) M. H. Kalos, D. Levesque, and L. Verlet, Phys. Rev. A **9**, 2178 (1974); b) P. A. Whitlock, D. M. Ceperley, G. V. Chester, and M. H. Kalos, Phys. Rev. B **19**, 5598 (1979).

26. R. Jastrow, Phys. Rev. **98**, 1479 (1955); R. B. Dingle, Philos. Mag. **40**, 573 (1949).

27. Z. W. Sun. P. J. Reynolds, R. K. Owen, and W. A. Lester, Jr., Theor. Chem. Acta **75**, 353 (1989).

28. P. Siegbahn and B. Liu, J. Chem. Phys. **68**, 2457 (1978).

29. C. E. Dykstra and W. C. Swope, J. Chem. Phys. **79**, 111 (1983).

Table 1. Geometries[a] and energies for the approach of $H_2(B)$ to $H_2(X)$

step	R'	L_1	L_2	$L_2(+)$	$L_2(-)$	D	Energy Lowering*
I	5-2.2	1.40	2.43	1.215	1.215	0.0	-0.91
II	2.2	1.40	2.43	1.215-1.93	1.215-0.5	0.715	-0.20
III	2.2	1.60	2.63	1.93-2.13	0.5	0.865	-0.20
IV	2.2-1.75	1.60	2.63	2.14	0.5	0.865	-1.18
V	1.75-1.55	1.60	2.73	2.23	0.5	0.915	-0.46
VI	1.55	1.60	3.13	2.23-2.63	0.5	1.115	-0.69
VII	1.50	1.70	3.23	2.63-2.73	0.5	1.165	-0.11

*Total energy lowering for the seven steps is 3.75 eV. Distances in a.u.; energies in eV.

[a]See Fig. 4 for a diagram defining the second-seventh table headings.

R' - distance between the midpoint of $H_2(X)$ and the point where $H_2(B)$ meets the $H_2(X)$.

L_1 - length of $H_2(X)$.

L_2 - length of $H_2(B)$.

$L_2(+)$ - length of $H_2(B)$ above the $H_2(X)$ plane.

$L_2(-)$ - length of $H_2(B)$ below the $H_2(X)$ plane.

D - magnitude of shift of $H_2(B)$ midpoint (above (+)/below (-)) plane of $H_2(X)$.

Table 2. CI[a] total energies of three lowest-lying states along the T-approach pathway for $H_2(B) + H_2(X)$

	Geometries[b]			Energies[c]		
#	L_1	L_2	L_3[d]	E_1	E_2	E_3
01	2.4300	1.4000	2.4000	-2.22600	-1.96950	-1.84546
02	2.4980	1.4309	2.2624	-2.21280	-1.97964	-1.84886
03	2.5542	1.6580	2.1276	-2.19672	-2.00442	-1.86340
04	2.6090	1.8072	2.0292	-2.17995	-2.01944	-1.86903
05	2.6640	1.9292	1.9438	-2.16423	-2.03169	-1.87339
06	2.7115	2.0325	1.8677	-2.15041	-2.04210	-1.87739
07	2.7528	2.1299	1.7985	-2.13818	-2.05115	-1.88108
08	2.8310	2.2829	1.6718	-2.11663	-2.06668	-1.88779
09	2.8955	2.4098	1.5653	-2.09978	-2.07845	-1.89327
10[e]	2.9503	2.5178	1.4713	-2.08778	-2.08610	-1.89775
11[e]	2.9840	2.6388	1.3703	-2.07027	-2.09714	-1.90038

[a]SDCI results based on MC reference molecular orbitals with DZP basis set.

[b]T-shape arrangement: H_cH_d bisects and is perpendicular to H_aH_b. L_1 is the length of H_aH_b and L_2 is the length of H_cH_d.

[c]Energies in a.u., 1 a.u. = 27.210 eV.

[d]L_3 is the distance from the midpoint of H_aH_b to the closer atom H_c. Distances in a.u.

[e]Curve crossing between the two geometries.

Table 3. MCSCF and QMC energies at several points along the crossing seam of the lowest-lying potential energy surfaces of pyramidal H_4.[a]

r (a.u.)	1.55	1.60	1.65	1.70	1.75
R (a.u.)	5.244	5.024	4.805	4.587	4.367
MCSCF	-1.9859	-1.9917	-1.9961	-1.9990	-2.0006
QMC	-2.0482(30)	-2.0504(28)	-2.0584(30)	-2.0531(31)	-2.0580(35)
ΔE (eV)	1.69	1.60	1.69	1.47	1.56

r (a.u.)	1.80	1.85	1.90	1.95	2.00
R (a.u.)	4.145	3.917	3.675	3.406	3.054
MCSCF	-2.0008	-1.9995	-1.9965	-1.9910	-1.9798
QMC	-2.0634(40)	-2.0621(26)	-2.0632(17)	-2.0633(21)	
ΔE (eV)	1.70	1.70	1.79	1.97	

[a] Energies in a.u. except where noted. 1 a.u. = 27.210 eV.

Table 1. Non-Adiabatic Coupling Matrix Elements

r(a.u.)	R(a.u.)	$< A' \mid E >^{a}_{1,2}$	$< A' \mid E >^{b}_{4,5}$	$< A' \mid E >^{c}_{3,6}$
1.70	4.0	1.90	0.29	0.0
1.70	3.8	2.10	0.31	0.0
1.80	4.22	3.18	0.52	0.0
1.80	4.4	4.59	0.86	0.0
1.80	4.6	8.10	1.60	0.0
1.90	4.6	13.79	2.67	0.0

[a]Non-adiabatic coupling induced by the doubly degenerate dissociative modes Q_1 and Q_2.

[b]Non-adiabatic coupling induced by the doubly degenerate bound modes Q_4 and Q_5.

[c]Non-adiabatic coupling induced by the totally symmetric modes Q_3 and Q_6.

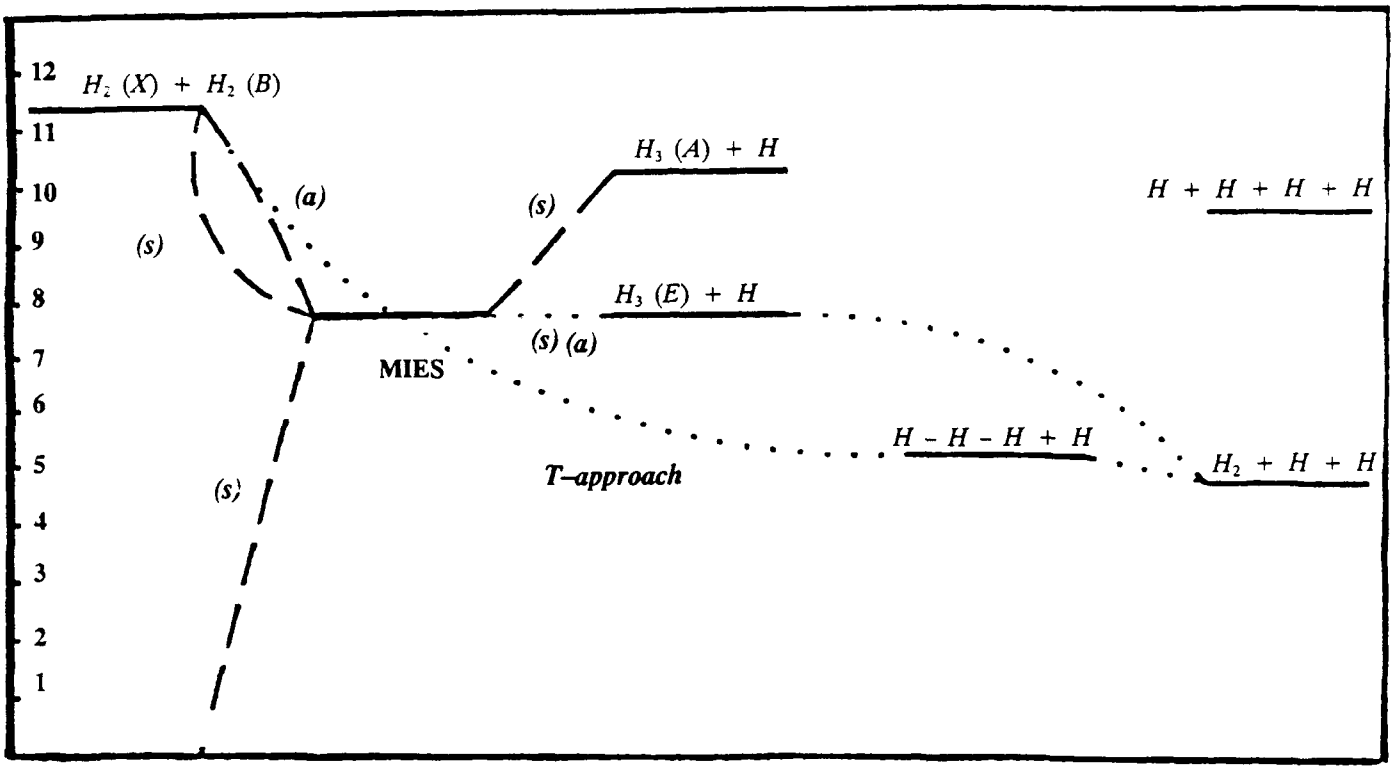

Figure 1
Correlation Diagram of Tetrahydrogen

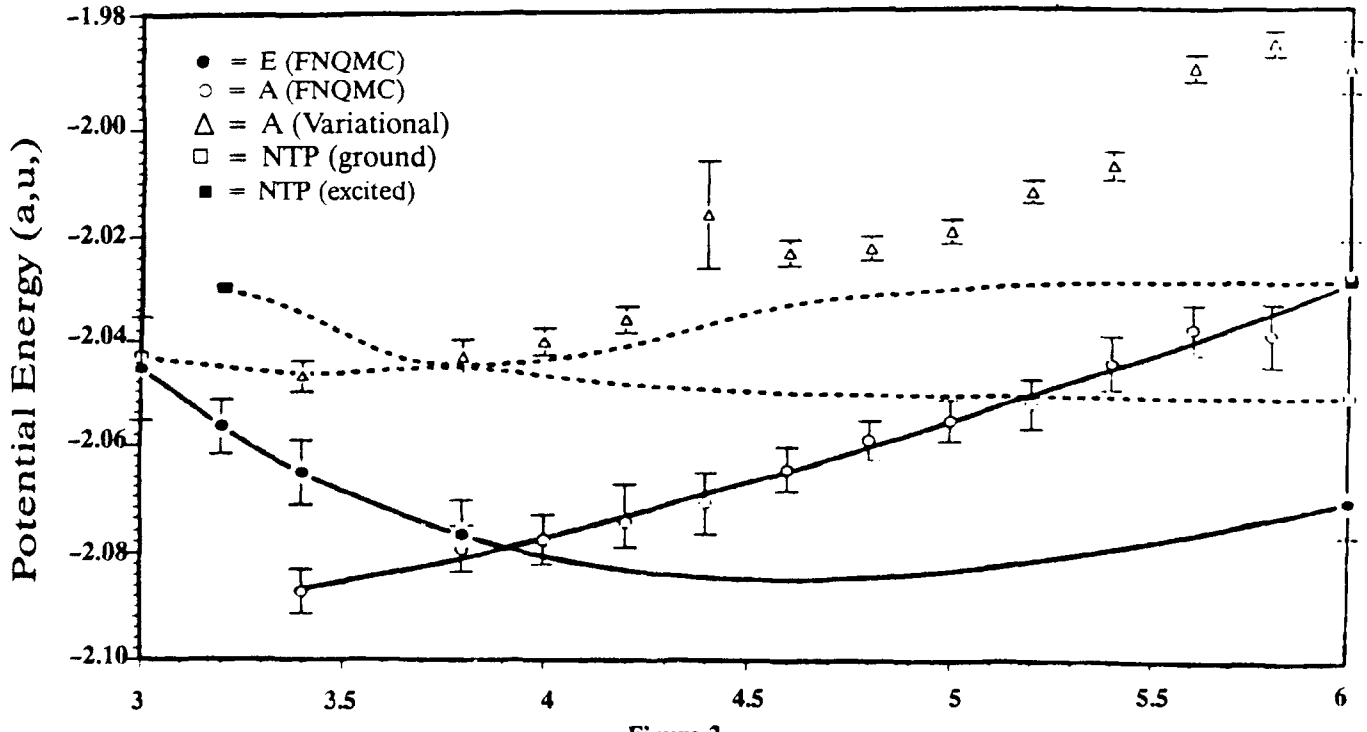

Figure 2

One–dimensional potential energy curves of pyramidal H_4 as a function of R for r = 1.70 a.u. where R is the separation from apex H to equilateral triangle base and r is the base side–length. Solid lines connect fixed node (FN) QMC calculated energies for the ^1E and $^1A_1$ states. The two dotted lines are the result from Ref. 1. The open triangles are VMC results.

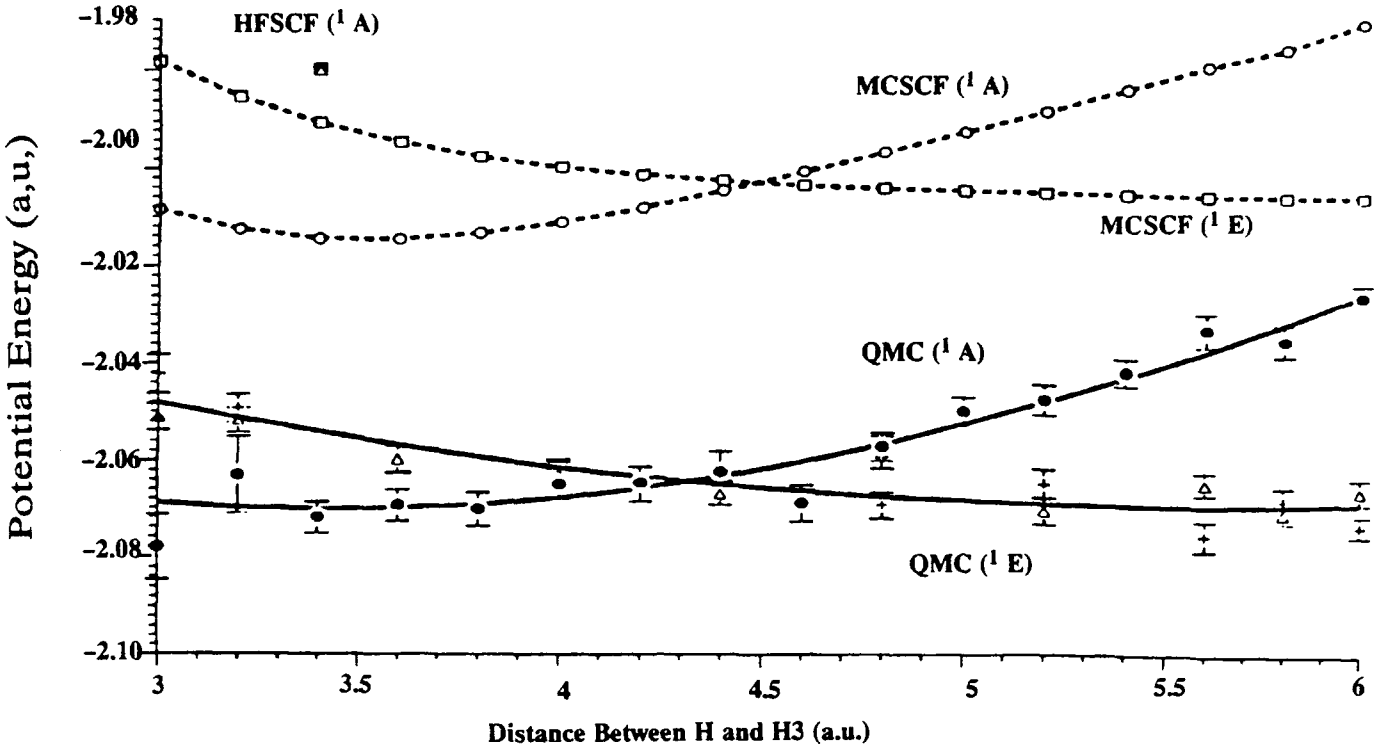

Figure 3

One–dimensional energy curves of pyramidal H_4 for r = 1.80 a.u. Solid lines connect FNQMC energies. Dotted lines connect MCSCF energies

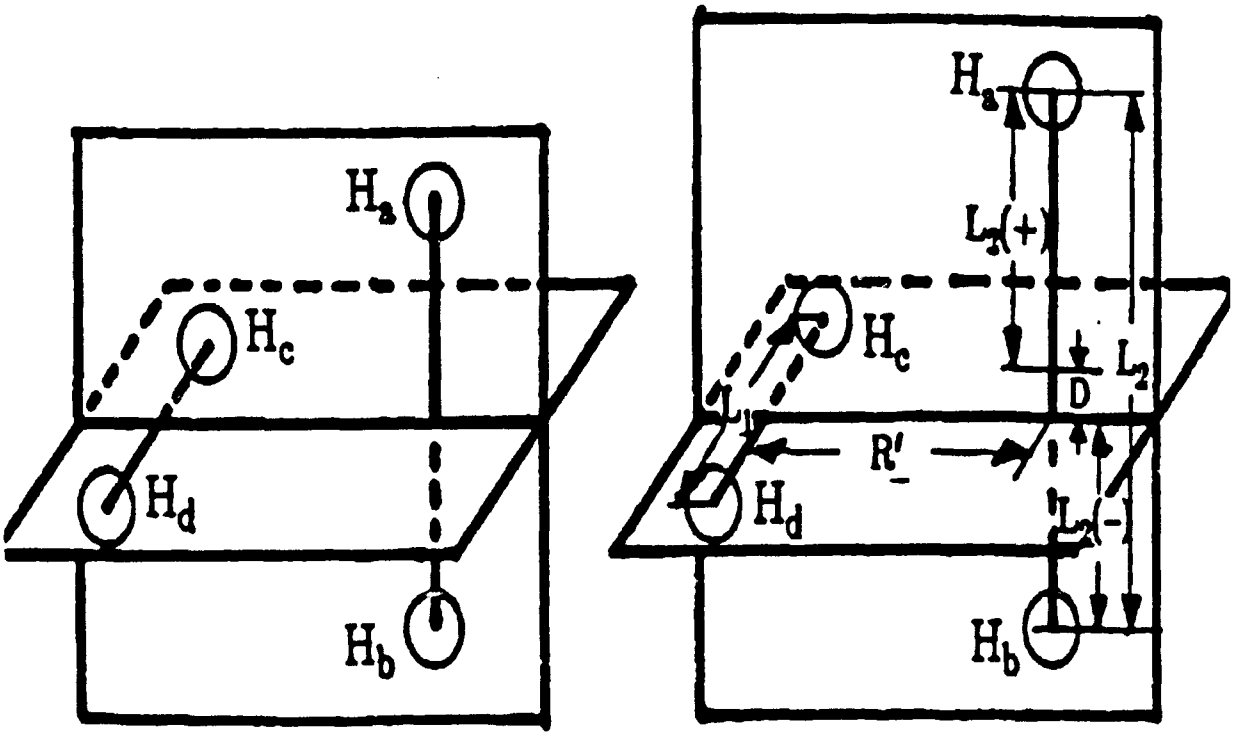

Figure 4

T–Approach Geometry for interaction of H_2 (B) with H_2 (X)

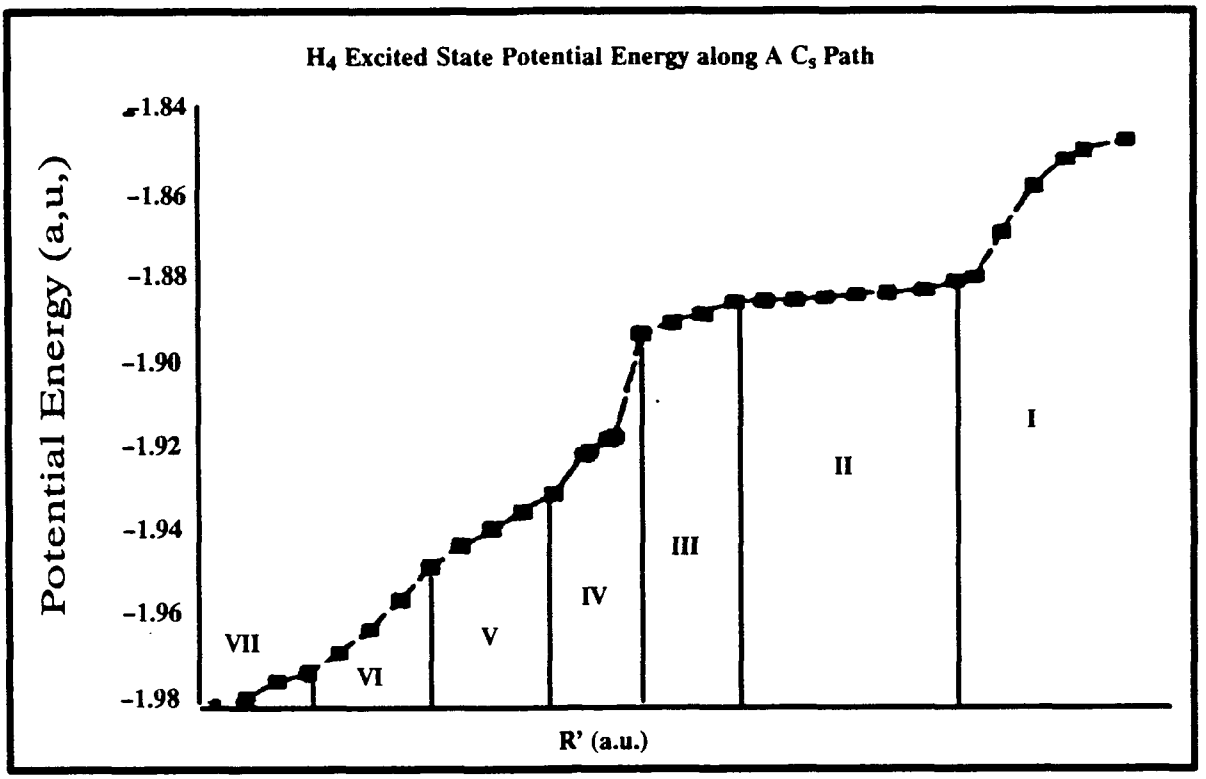

Figure 5
Plot of Total Energies Corresponding to the Pathway Presented in Table 1.

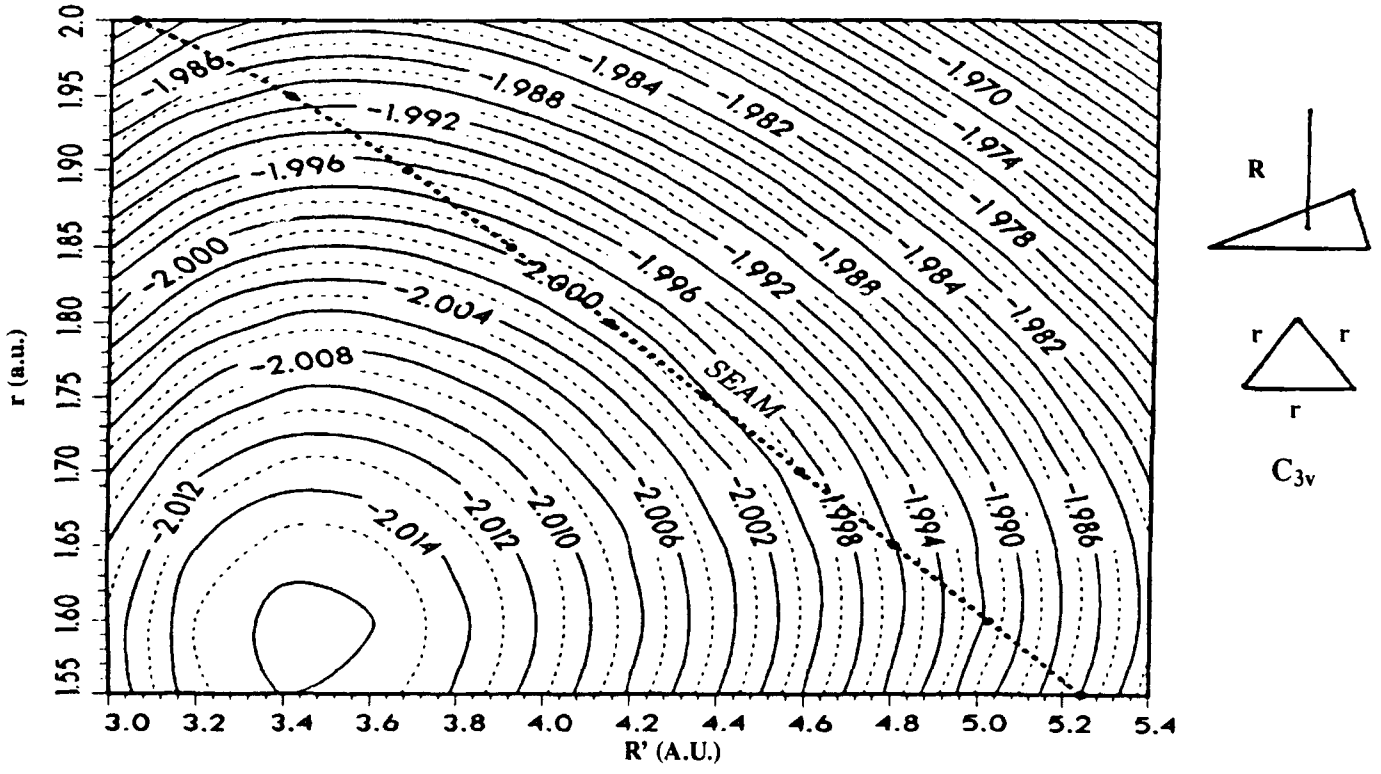

Figure 6
Contour map of $^1A_1$ potential energy surface of pyramidal H_4. R is the distance between apex H and triangle base H_3. r is the side length of H_3. The dotted line is the crossing seam of the $^1A_1$ state and the doubly degenerate ^1E state.

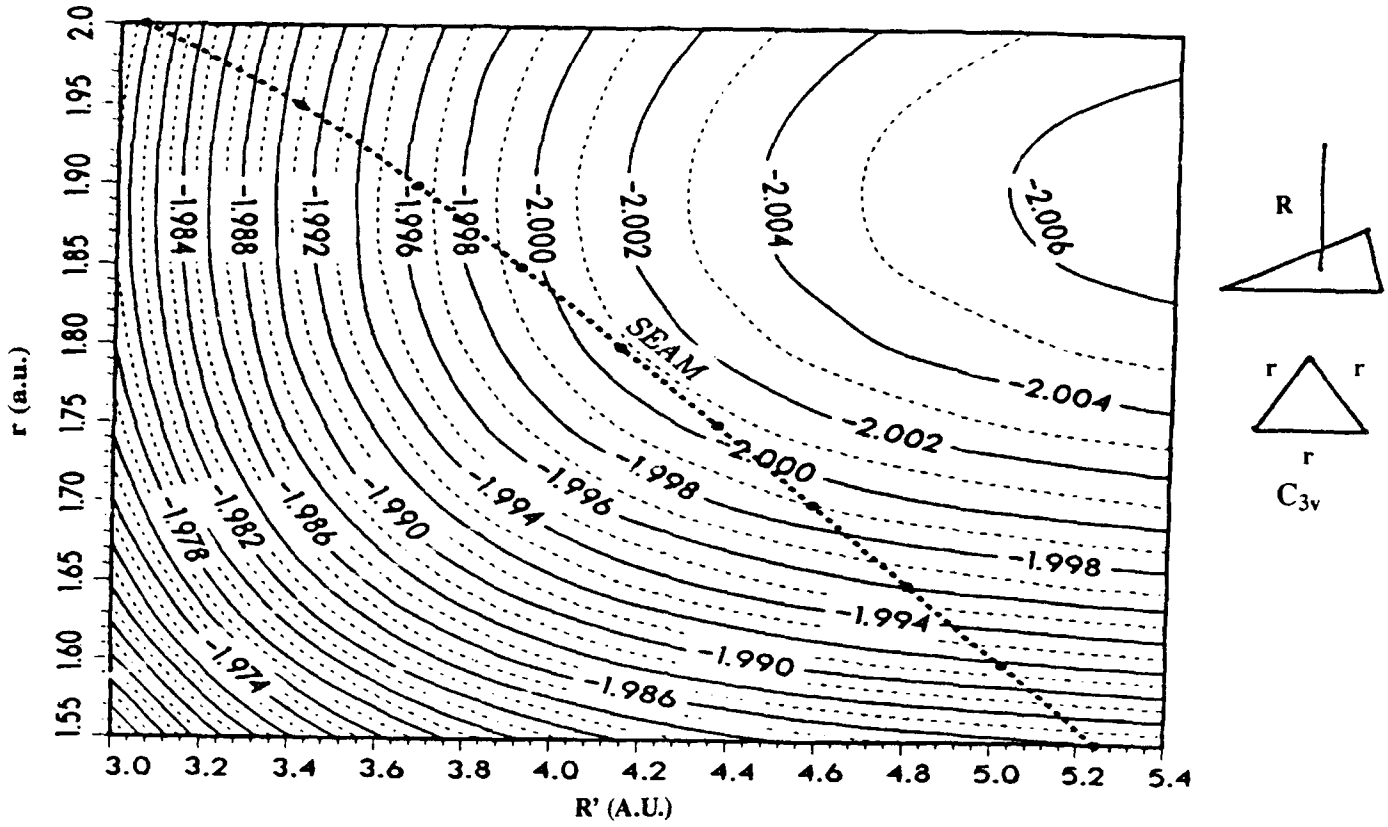

Figure 7

Same as Figure 5 except the potential energy surface is for the doubly degenerate ^1E state.

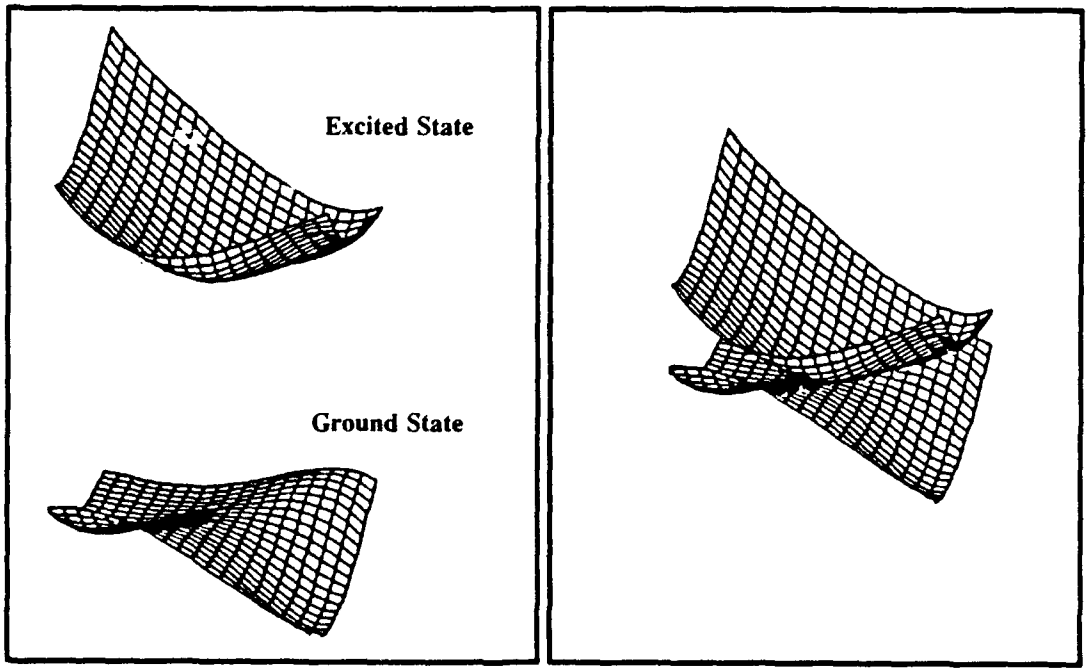

Figure 8

Perspective view of two of the three lowest-lying pes's of tetrahydrogen in C_s symmetry, see text.

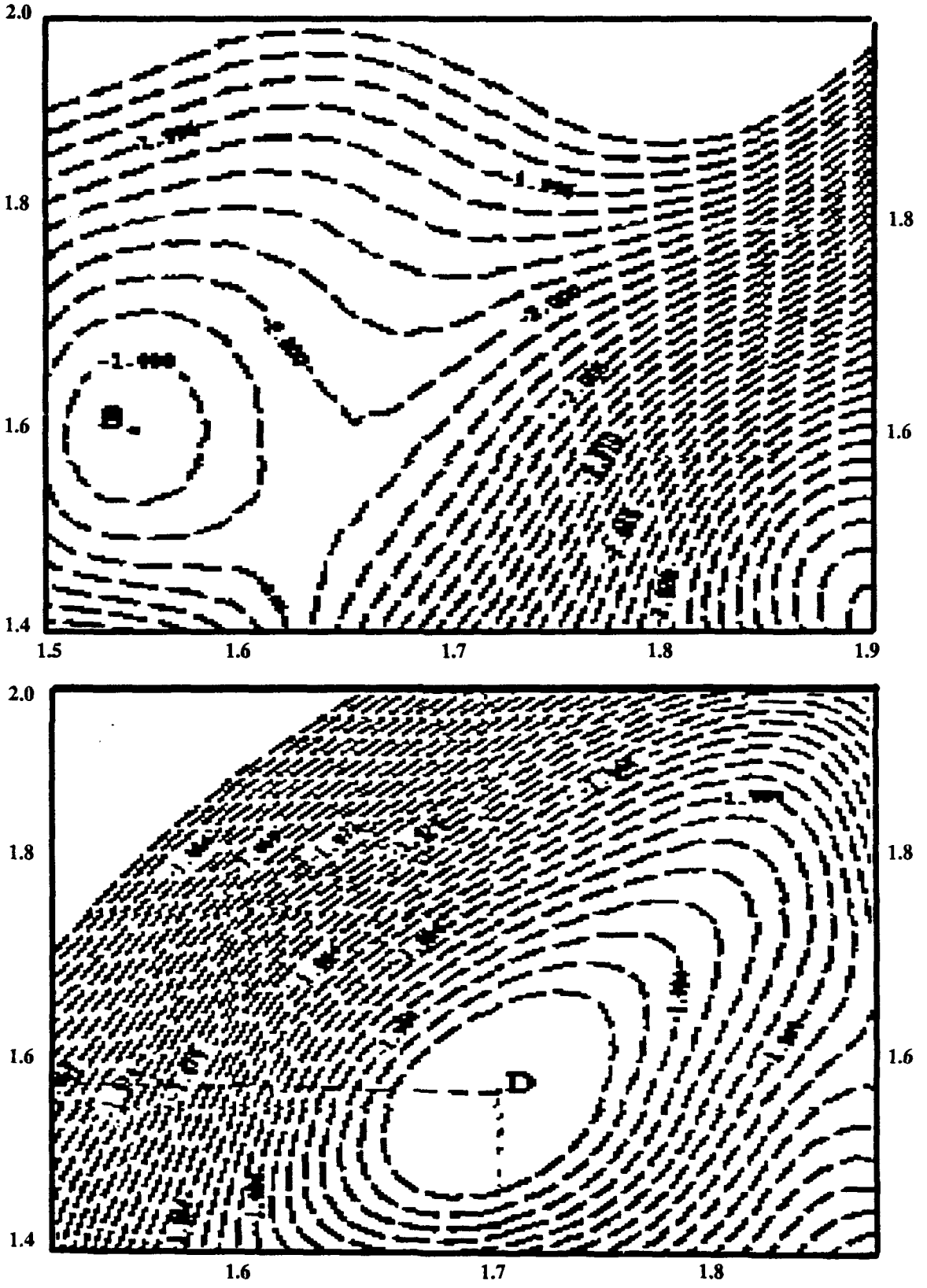

Figure 9

Contour map for R = 4.0 a.u. as a function of a and b; see Figure 9 for definition.
Upper panel: ground state Lower panel: excited state.

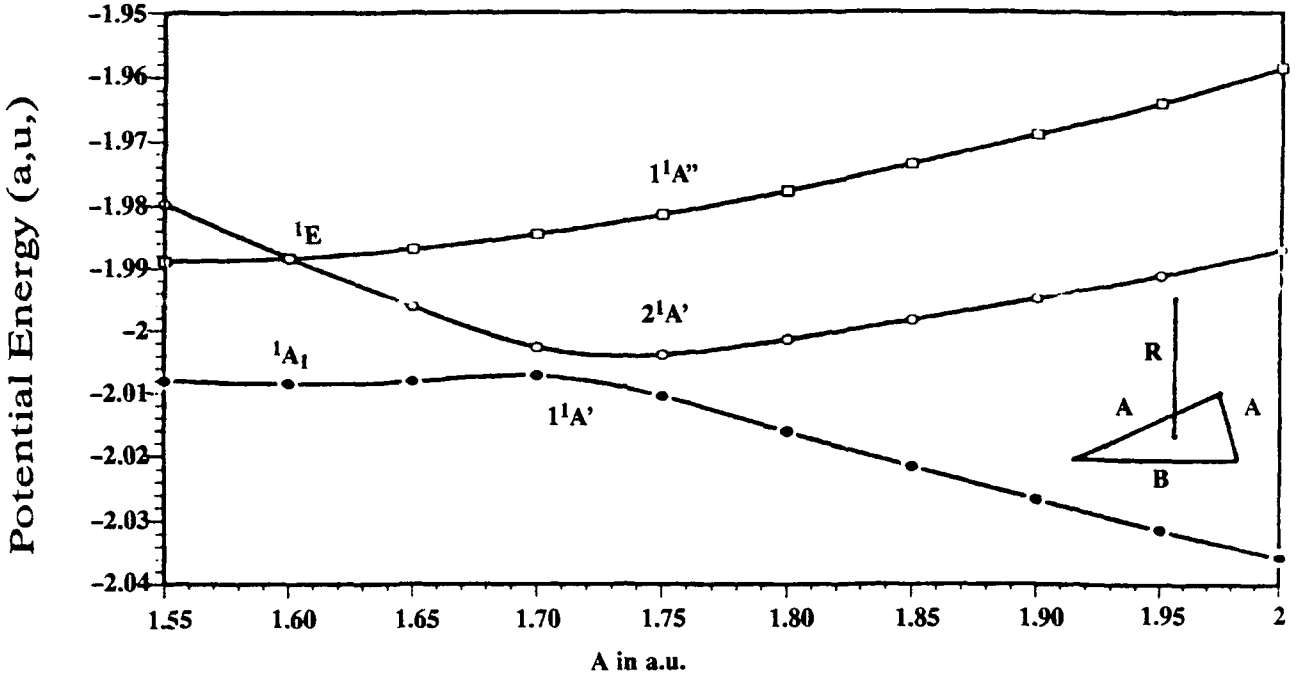

Figure 10

Three lowest–lying potential energy curves for pyramidal H_4 with isoceles triangle base as a function of A, the length of the two equal sides for R = 4.2 a.u. and B = 1.6 a.u. The ^1E curve splits into two branches for A ≠ B, and the symmetric branch 2 $^1A'$ interacts with the ground state $1^1A'$.

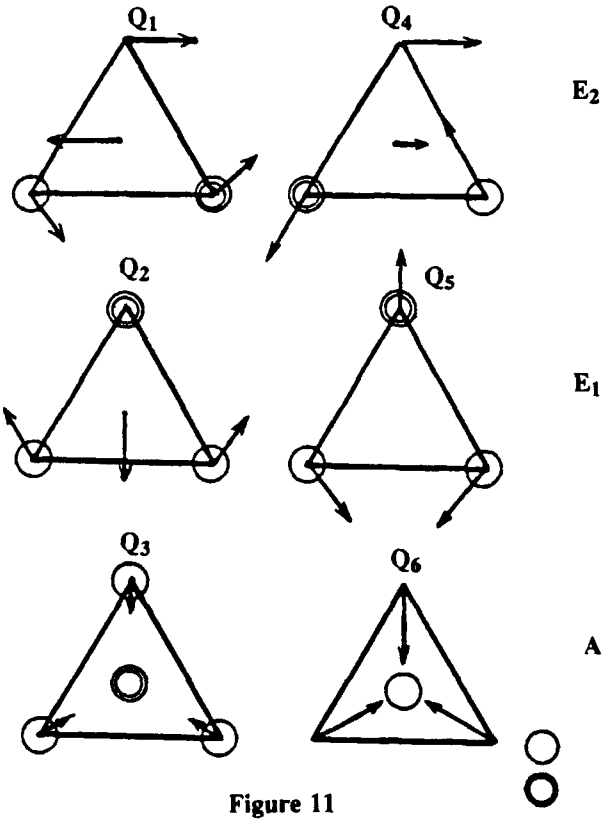

Figure 11
Normal modes of H_4

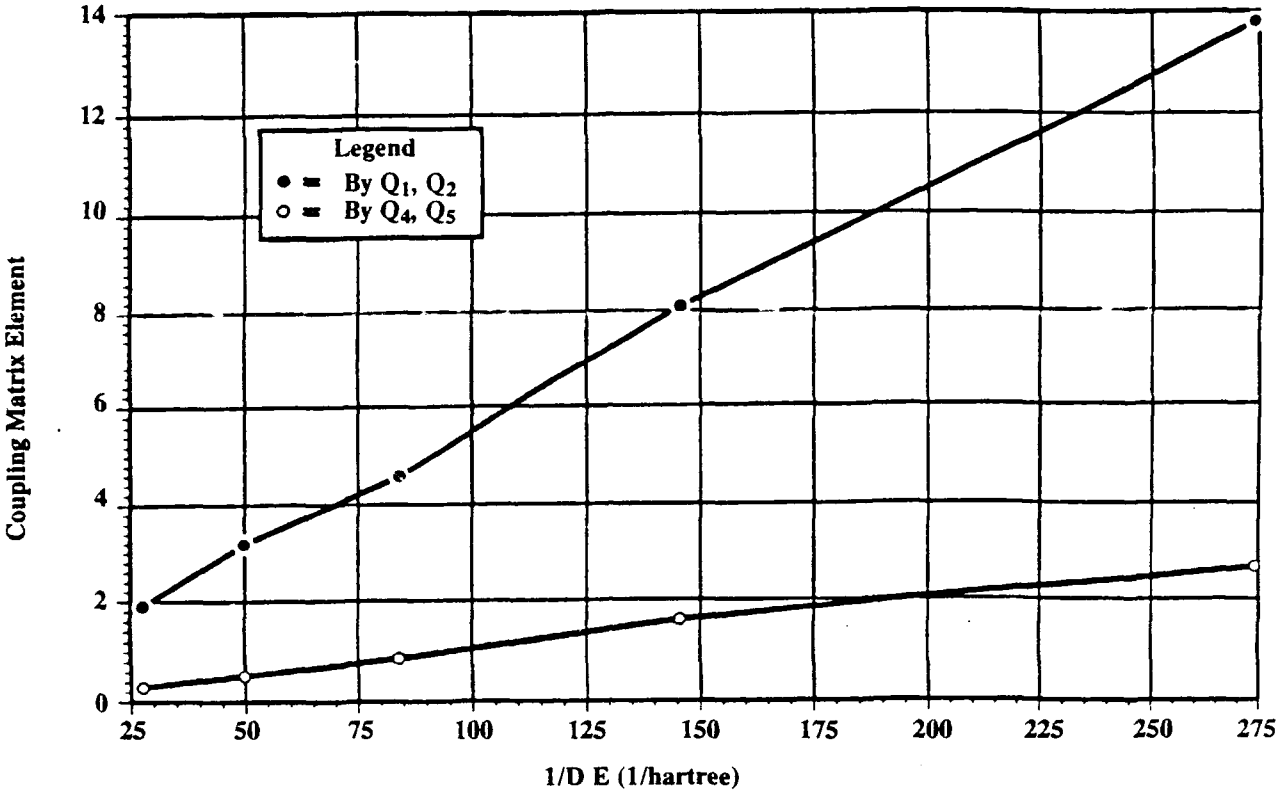

Figure 12

Calculated nonadiabatic coupling matrix elements at five geometries vs the inverse of the energy difference between the pes's.

PART B: QUANTUM MONTE CARLO STUDY OF THE 1 $^1A'$ and 2 $^1A'$ POTENTIAL ENERGY SURFACES He + H_2

I. Introduction

There is much theoretical and experimental interest in the reactions of atoms with electronically excited molecules. The He + H_2 system is particularly suitable for theoretical studies because of its simplicity: four electrons and three nuclei. Considerable effort has been made to understand the quenching of $H_2(B\ ^1\Sigma_u^+)$ by He[1-11] and its large effective energy transfer cross section. After unsuccessful attempts to find an avoided crossing along C_{2v} and $C_{\infty v}$ approaches,[4] Farantos *et al.*[5] located an avoided crossing for general C_s approach which shed light on the quenching process. Subsequent construction of analytical *ab initio* potential-energy surfaces for the 1 $^1A'$ and 2 $^1A'$ states[6] made possible dynamics studies.[7-10] However, Farantos's quenching cross sections were much smaller than the experimental values.[7] Later Yarkony *et al.*[10-11] extended study of the avoided crossing region using a second-order CI method and found that there is actually a crossing seam between these pes's. This development holds new promise for understanding electronic quenching in the subject system.

The QMC method[12-14] is characterized by its high accuracy and simplicity in the calculation of energies of small molecules. It is of interest to ascertain the capability of the QMC to treat the He + H_2 system which, because of its small number of electrons, is

an ideal candidate for QMC studies. On the other hand, these studies are also challenging because the stochastic nature of QMC makes it difficult to obtain the high precision which is required for small interaction energies even though the QMC method routinely yields total electronic energies lower than basis set methods. In an attempt to minimize these considerations, special procedures were introduced in this study including total wavefunction optimization and the use of averages over independent calculations.

In Sec. I we describe the wavefunctions and optimization and computational methods. In Sec. III we present the results and discussion. Section IV contains our summary and conclusions.

II. Method

A. QMC approach

The VMC method, which evaluates the energy expectation value according to the trial wavefunction distribution Ψ_T^2, is much more efficient than diffusion QMC because QMC has serious sample self-correlations for small time-steps. However, the VMC energy depends strongly on the quality of the trial function and it is difficult to guarantee the same quality at different geometries. In this study we use the fixed-node[14] QMC approach because it has the advantages of simplicity, stability, and high accuracy. We note that the fixed-node depends on the nodal structure of Ψ_T.

B. Wavefunction and optimization

Double-zeta-plus-polarization basis sets of atom-centered Slater-type orbitals were used. The orbital exponents are: ζ_{1s} =

1.147, $\zeta_{1s'}$ = 0.349, ζ_{2px} = ζ_{2py} = 1.200 for the atom-centered functions on H and ζ_{1s} = 1.446, $\zeta_{1s'}$ = 2.862, ζ_{2px} = ζ_{2py} = 1.200 for atom-centered functions on He.

The trial wavefunctions Ψ_T can be expressed as

$$\Psi_T = \Phi(1,2,3,4) S_e[\{r_{ij}\}] S_n[\{r_{i\alpha}\}] \quad , \tag{1}$$

For the 1 ^{1}A' state (closed shell, the configuration is $\psi_1^2\psi_2^2$) we have:

$$\Phi(1,2,3,4) = (\psi_1(1)\psi_2(2) - \psi_2(1)\psi_1(2))(\psi_1(3)\psi_2(4) - \psi_1(4)\psi_2(3)) \quad , \tag{2}$$

For the 2 ^{1}A' state (open shell, the configuration is $\psi_1^2\psi_2\psi_3$) we have:

$$\Phi(1,2,3,4) = (\psi_1(1)\psi_2(2) - \psi_2(1)\psi_1(2))(\psi_1(3)\psi_3(4) - \psi_1(4)\psi_3(3))$$

$$+ (\psi_1(1)\psi_3(2) - \psi_3(1)\psi_1(2))(\psi_1(3)\psi_2(4) - \psi_1(4)\psi_2(2)) \quad , \tag{3}$$

The electron-electron correlation function S_e in this study was chosen to have the form[16]

$$S_e[\{r_{ij}\}] = exp[-b \sum_{r_{ij}} exp(-a_1 r_{ij} + a_2 r_{ij}^2)] \quad , \tag{4}$$

In order to reduce the variance in the local energy, $E_L \equiv \Psi_T^{-1} H \Psi_T$, the parameter a is set to 0.5/b. This choice removes the singularity in E_L due to the coalescence of electrons of opposite spin. (Satisfying the cusp condition for electrons of like spin is

not important for present purposes because $\Psi_T \rightarrow 0$ as such electrons coalesce.) This leaves two parameters to be determined. Equation (4) is both easy to evaluate and yields a good description of electron correlation.[15]

The electron-nuclear correlation function, S_n, further increases the flexibility of the trial function and complements the determinant in satisfying the electron-nuclear cusp condition. The form used here is the familiar Jastrow form

$$S_n[\{r_{i\alpha}\}] = exp\left[\sum_{i,\alpha} \frac{-\lambda r_{i\alpha}}{1 + \nu r_{i\alpha}}\right] . \qquad (5)$$

The trial function specifies the nodal boundaries which ultimately determine the accuracy of computed energies, and serves as a guiding function for importance sampling during the random walk. High quality trial functions are essential not only to enhance the convergence rate of the computation but also to reduce the time-step bias in the fixed-node QMC procedure.[16] In order to improve the quality of the trial function, a fixed-sample optimization is performed before each product calculation. Even though a full scale optimization of all trial function parameters, both for the basis set and correlation functions, has been proven to be useful for both VMC and QMC energies using single determinant wavefunctions,[16] it is still in question for QMC energies using multideterminant wavefunctions because the optimization procedure may degrade the nodal structure of multideterminant wavefunctions.[17]

Since multideterminant wavefunctions were used in the QMC calculations reported here, in order to avoid nodal structure degradation, we only optimized correlation function parameters and left the basis set parameters unchanged. Since correlation functions are nodeless, changes of parameters of those functions during optimization does not affect the nodal structure of Ψ_T nor the QMC energies. However, optimized correlation parameters can still play a role in reducing energy variance, time-step bias, and in satisfying cusp conditions.

C. Computational procedure

The QMC energies are computed at points on the minimum energy pathway of Farantos's analytic pes for selected orientations. In this work r is the H_2 internuclear separation, R is the distance from He to the center of mass of H_2, and θ is the orientation angle formed by r and R. Nuclear geometry is specified by the ordered triple (R,r,θ) with R and r in atomic units, and θ in degrees.

For each geometry, we used the HONDO program to obtain the MO coefficients, combined the resulting independent particle function with the correlation function, and then performed an unoptimized VMC calculation to create a set of configurations for use in optimization. From 1,000 to 1,500 sample points were used in the fixed-sample optimization procedure followed.[16] The eight parameters of the correlation functions were optimized, and the resulting wavefunction used in a VMC calculation to yield 1,000 configurations which were divided equally into ten groups. These

ten sets of configurations were then used to perform ten independent QMC calculations.

The final QMC energy is the average value of these ten calculations. Using the average value of the independent runs is helpful in removing sample dependence and self-correlations. Trial function optimization appears to be a useful method of reducing time-step bias for QMC calculations. Figure 1 shows QMC energies vs time-step from which one sees that the bias vanishes for $\tau < 0.01$. On this basis all of the QMC calculations were carried out with $\tau = 0.005$. Including wavefunction optimization, the calculations for each geometry took approximately two hours of CPU time on a CRAY X-MP using vectorized codes.

III. Result and Discussion

The QMC energies for the minimum energy pathways for $\theta = 0°$, 30°, 45°, and 90° are listed in Tables I and II. There are intersections between the 1 ^{1}A' and 2 ^{1}A' pes's around (1.75, 4.13, 45) and (1.75, 5.74, 30). Since the pes's should be continuous the interactions must extend over a considerable region. (On the other hand Farantos shows the closest approach of the two surfaces to be 5 kcal/mol at (1.788, 4.44, 29.88).) This finding supports the extended region of crossing of the two surfaces found by Yarkony *et al.*[10,11] and provides an explanation for the high quenching rate of $H_2(B\ ^1\Sigma_u^+)$ by He. Furthermore, the present calculations show the energy of the 2 ^{1}A' state even lower than that of the 1 ^{1}A' state at (1.75, 4.13, 45). The conditions for intersections of pes's of

polyatomic molecules have been discussed extensively.[18-22] The intersection of two surfaces having the same symmetry is allowed for polyatomic molecules. As Manaa *et al.*[11] have indicated, such intersections may play an important role in multistate electronically nonadiabatic processes.

In general, the present QMC energies are significantly lower than the energies obtained in previous studies. In particular, our computed well depth for the 2 ^{1}A' state is about 50 kcal/mol which is to be compared with previous values of 35 kcal/mol[6] and 39 kcal/mol.[10] As a check on the accuracy of the QMC energies we compared results at the asymptotic limit. The experimental value for the ground state of He is −2.9037h,[23] the best computed energies for $H_2(B\ ^1\Sigma_u^+)$ and $H_2(X\ ^1\Sigma_g^+)$ at r = 2.43 bohr are respectively −0.7567h[24] and −1.0999h.[25] We can infer that the exact energies for 2 ^{1}A' and 1 ^{1}A' states asymptotically should be −3.6604h and −4.0036h, respectively. For comparison, Yarkony[11] obtained −3.6501h and −3.9962h; Farantos's value[6] for E(2 ^{1}A') is −3.6499h; our QMC results are −3.6591(14)h and −4.0033(11)h.

The data in Tables 1 and 2 give a rough picture of the shape of the pes for the 2 ^{1}A' state. At 45° the minimum energy path (MEP) is initially at r = 2.4a_0 and changes only slightly up to R = 3.0 a_0. Around (1.75, 4.1, 45) there is a minimum which is in the vicinity of the intersection with the 1 ^{1}A' surface. There is a barrier on the MEP before the minimum and as soon as the approaching He overcomes the barrier it is quenched to the 1 ^{1}A'

state. Farantos's calculations predict this barrier to be 5.26 kcal/mol at (1.5, 4.0, 45), but Yarkony claims a barrier of 1.49 kcal/mol at (2.65, 2.52, 64.178). The recent experimental estimate of the barrier by Pibel *et al.*[26] is only 0.715 kcal/mol. It is clear that He atom must have enough energy and proper orientation to pass the barrier and decay to 1 ^{1}A' state.

At present, there is no QMC technique to locate the saddle point aside from estimates using other *ab initio* techniques. Using Farantos's location (30, 2.4, 45), our QMC energy is −3.6396(9)h and the corresponding barrier is 12.2 kcal/mol. Using Yarkony's location (2.65, 2.52, 64.178) we obtained −3.6469(12)h and a barrier of 7.6 kcal/mol.

References

1. D. L. Atkins, E. H. Fink, and C. B. Moore, J. Chem. Phys. **52**, 1604 (1970).
2. E. H. Fink, D. L. Atkins, and C. B. Moore, J. Chem. Phys. **56**, 900 (1972).
3. H. F. Schaefer, D. Wallach, and C. F. Bender, J. Chem. Phys. **56**, 1219 (1972).
4. (a) J. Römelt, S. D. Peyerimhoff, and R. J. Buenker, Chem. Phys. **34**, 403 (1978); (b) J. Römelt, S. D. Peyerimhoff, and R. J. Buenker, Chem. Phys. **41**, 133 (1979).

5. S. C. Farantos, G. Theodorakopoules, and C. A. Nicolaides, Chem. Phys. Lett. **100**, 263 (1983).

6. S. C. Farantos, J. N. Murrell, and S. Carter, Chem. Phys. Lett. **108**, 367 (1983).

7. S. C. Farantos, Mol. Phys. **54**, 835 (1985).

8. R. M. Grimes, W. A. Lester, Jr., and M. Dupuis, J. Chem. Phys. **84**, 5437 (1986).

9. P. Pernot, R. M. Grimes, W. A. Lester, Jr., and C. Cerjan, Chem. Phys. Lett. **163**, 297 (1989).

10. J. K. Perry and D. R. Yarkony, J. Chem. Phys. **89**, 4945 (1988).

11. M. R. Manaa and D. R. Yarkony, J. Chem. Phys. **93**, 4473 (1990).

12. M. H. Kalos, Phys. Rev. **128**. 1791 (1972); **A2**, 250 (1970); J. B. Anderson, J. Chem. Phys. **63**, 1499 (1975); **65**, 4121 (1976).

13. D. M. Ceperley and M. H. Kalos, *Monte Carlo Methods in Statistical Physics,* ed. by K. Binder (Springer-Verlag, New York, 1979); *Quantum Monte Carlo Methods,* ed. by M. Suzuki (Springer-Verlag, New York, 1987); W. A. Lester, Jr. and B. L. Hammond, Ann. Rev. Phys. Chem. **41**, 283 (1991).

14. J. B. Anderson, J. Chem. Phys. **63**, 1499 (1975); D. M. Ceperley and B. J. Alder, Phys. Rev. Lett. **45**, 566 (1980); D. M. Ceperley, *The Stochastic Solution of the Many-Body Schödinger Equation for Fermions in Recent Progress in Many-Body Theories,* ed. by J. G. Zabolitzky, M. de Liano, M. Fortes, and J. W. Clark (Springer, Berlin, 1981), p. 262-269; J. M. Moskowitz, K. E. Schmitt, M. A. Lee, and M. H. Kalos, J. Chem. Phys. **77**, 349 (1982); P. J. Reynolds, D. M. Ceperley, B. J. Alder, and W. A. Lester, Jr , J. Chem. Phys. **77**, 5593 (1982).

15. Z. Sun. P. J. Reynolds, R. K. Owen, and W. A. Lester, Jr., West Coast Theoretical Chemistry Conference, Santa Barbara, CA, April 1986. Also, Theor. Chim. Acta **75**, 353 (1989).

16. Z. Sun, S.-Y. Huang, R. N. Barnett, and W. A. Lester, Jr., J. Chem. Phys. **93**, 3326 (1990).

17. Z. Sun, R. N. Barnett, and W. A. Lester, Jr., West Coast Theoretical Chemistry Conference, Mountain View, CA, March 1991.

18. G. Herzberg and H. C. Longuet-Higgins, Discussions Faraday Soc., **35**, 77 (1963).

19. C. M. Meerman-van Benthem, A. H. Huizer, and J. J. C. Mulder, Chem. Phys. Lett. **51**, 93 (1977).

20. G. J. Hatton, W. L. Lichten, and N. Ostrove, Chem. Phys. Lett. **40**, 437 (1976).

21. T. Carrington, Accts. Chem. Res. **7**, 20 (1974).

22. E. Ohrendorf, L. S. Cederbaum, and H. Köppel, Chem. Phys. Lett. **151**, 273 (1988).

23. See, for example, I. N. Levine, *Quantum Chemistry* (Allyn and Bacon, Boston, 1983).

24. W. Kolos and L. Wolniewicz, Can. J. Phys. **53**, 2189 (1975).

25. W. Kolos and L. Wolniewicz, J. Chem. Phys. **43**, 2429 (1965).

26. C. D. Pibel, K. L. Carleton, and C. B. Moore, J. Chem. Phys. **93**, 323 (1990).

Table 1. QMC Total Energies of HeH_2 for $\theta = 0°$, 30°, 45°.*

$\theta(°)$	R	r	E(1A')†	E(2A')†
0.00	5.0000	2.2170	-4.0185(11)	-3.6430(13)
	5.0000	2.4300	-3.9987(08)	-3.6428(14)
	5.5220	2.2900	-4.0148(09)	-3.6486(09)
	5.9855	2.3260	-4.0117(07)	-3.6505(07)
	6.4500	2.3620	-4.0075(12)	-3.6516(09)
	6.9700	2.4000	-4.0043(12)	-3.6560(14)
	10.000	2.4300	-4.0039(10)	-3.6552(13)
30.00	0.0580	3.9060	-3.8151(16)	-3.6036(11)
	0.4930	4.0870	-3.8007(10)	-3.6438(13)
	1.0140	4.5220	-3.7729(12)	-3.6925(18)
	1.1390	4.7750	-3.7406(18)	-3.7025(10)
	2.0000	5.1740	-3.7073(18)	-3.7082(15)
	2.4920	4.7250	-3.7163(10)	-3.6745(19)
	3.0145	4.4640	-3.7874(09)	-3.6748(12)
	4.0000	2.1740	-4.0157(09)	-3.6389(12)
	4.5070	4.8700	-3.8214(14)	-3.7259(14)
	4.9860	2.2900	-4.0120(09)	-3.6476(10)
	7.0140	2.4060	-4.0048(09)	-3.6554(15)
45.00	0.0290	3.9130	-3.8165(16)	-3.6020(14)
	0.4900	4.0000	-3.8028(10)	-3.6333(13)
	1.0000	4.0870	-3.7690(12)	-3.6807(17)
	1.5000	4.0000	-3.7310(13)	-3.7154(10)
	1.5900	4.1300	-3.7317(13)	-3.7268(11)
	1.7500	4.1300	-3.7267(10)	-3.7408(09)
	2.0000	4.1100	-3.7519(10)	-3.7242(12)
	2.4900	4.1300	-3.8103(16)	-3.7112(17)
	3.0000	4.1680	-3.8529(12)	-3.6747(19)
	3.0000	2.4000	-3.9637(08)	-3.6396(10)
	3.5070	2.2550	-4.0002(07)	-3.6431(14)
	4.0000	2.2550	-4.0190(09)	-3.6475(11)
	4.5800	2.3190	-4.0084(08)	-3.6518(12)

*Energies are in hartrees and distances in bohr.

†The parenthetical quantity is the standard deviation.

Above two notes are also applicable to Table 2.

Table 2. QMC Total Energies of HeH_2 for θ = 45°, 65°, and 90°

$\theta(°)$	R	r	E(1A')	E(2A')
45.00	5.0000	2.4700	-3.9960(07)	-3.6522(14)
	5.0140	2.3770	-4.0052(10)	-3.6520(10)
	5.5000	2.4600	-3.9985(07)	-3.6534(15)
	6.0000	2.4500	-4.0003(18)	-3.6550(18)
	6.0000	2.4060	-4.0038(09)	-3.6556(08)
	7.0000	2.4340	-4.0029(08)	-3.6563(10)
	6.5000	2.4400	-4.0016(20)	-3.6554(18)
	20.000	2.4300	-4.0037(8)	-3.6591(14)
65.00	0.0500	3.8200	-3.8108(10)	-3.6028(15)
	0.5000	3.8100	-3.8007(14)	-3.6140(19)
	1.0000	3.7900	-3.7824(14)	-3.6503(15)
	1.5000	3.6000	-3.7438(18)	-3.7117(13)
	2.0000	3.1900	-3.8213(12)	-3.6572(14)
	2.5000	2.8700	-3.9010(21)	-3.6443(12)
	3.0000	2.5900	-3.9565(08)	-3.6483(13)
	3.5000	2.4200	-3.9904(08)	-3.6544(08)
	4.0000	2.4300	-3.9953(13)	-3.6567(09)
	4.5000	2.4300	-4.0012(11)	-3.6545(10)
	5.0000	2.4300	-4.0018(09)	-3.6559(10)
	6.0000	2.4300	-4.0023(12)	-3.6580(08)
	7.0000	2.4300	-4.0011(09)	-3.6571(08)
	8.5000	2.4300	-4.0022(12)	-3.6581(09)
	12.000	2.4300	-4.0029(09)	-3.6566(10)
90.00	0.0500	3.9130	-3.8164(13)	-3.6030(14)
	0.5000	3.7400	-3.8009(14)	-3.5989(14)
	1.0000	3.3910	-3.7655(10)	-3.5997(14)
	1.2610	3.2460	-3.7433(08)	-3.6003(10)
	1.4930	3.1300	-3.7223(12)	-3.6060(18)
	1.7540	2.9850	-3.7974(11)	-3.6203(14)
	2.0000	2.8400	-3.8481(14)	-3.6353(12)
	2.3480	2.4640	-3.9124(17)	-3.6463(11)
	3.0140	2.1740	-3.9984(11)	-3.6540(08)
	3.5070	2.2320	-4.0063(11)	-3.6580(10)
	4.0000	2.3480	-4.0048(09)	-3.6594(13)
	4.5220	2.4930	-3.9946(12)	-3.6586(13)
	4.9850	2.5210	-3.9949(10)	-3.6560(08)
	5.9710	2.4930	-3.9964(09)	-3.6583(11)
	8.0000	2.4340	-4.0024(09)	-3.6567(11)

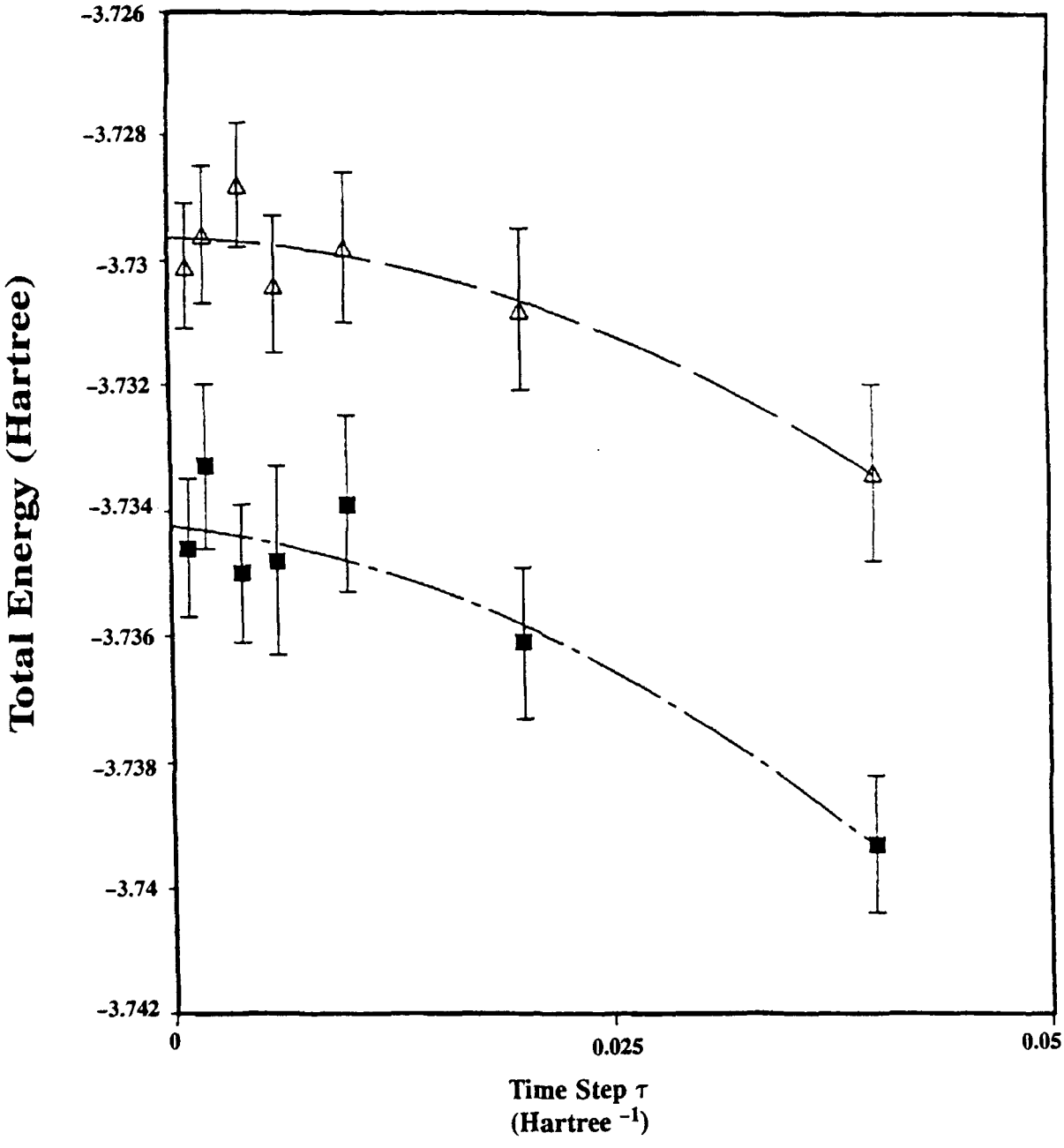

Figure 1

The fixed-node QMC total energy at geometry (1.59, 4.18, 45) vs time step τ